

Microstructure and Properties of AlCoCrFeNiB_x($x=0, 0.1, 0.25, 0.5, 0.75, 1.0$) High Entropy Alloys

Chen Qiushi, Dong Yong, Zhang Junjia, Lu Yiping

Dalian University of Technology, Dalian 116024, China

Abstract: The influences of B element on the microstructure and properties of AlCoCrFeNiB_x ($x=0, 0.1, 0.25, 0.5, 0.75, 1.0$, mol ratio) high entropy alloys were investigated. The AlCoCrFeNi high entropy alloy exhibits equiaxed grain morphology, and then turns to dendritic structures when B content $x=0.1$. The spinodal decomposition microstructure can be clearly observed in equiaxed grains. When $x>0.1$, both of the dendrite and the spinodal decomposition microstructure gradually disappear, but much borides form instead. The transformation is attributed to the high negative mixing enthalpy of Cr-B and Co-B. The microstructures of AlCoCrFeNiB_x high entropy alloys change from B2+bcc structures to B2+bcc+fcc structures, and finally formed B2+bcc+fcc and borides mixing structures with the increased B elements. The hardness HV declines from 4860 to 4607 MPa, then rises to 6157 MPa with the addition of B element. The lowest hardness value is obtained when $x=0.1$. The compressive fracture strength shows a distinct decrease with B addition. The maximum compression strength is 2227 MPa when $x=0.25$. But when x reaches 0.75, the samples fracture during the elastic deformation due to the formation of hard and brittle borides. The coercive forces and the specific saturation magnetizations of the alloys decrease as the contents of B element increase. The decreasing coercive forces show a better soft magnetic behavior.

Key words: high-entropy alloys; microstructures; microhardness; compressive properties; magnetic behavior

Conventional alloy-design strategy is mainly based on one or two elements as the principal components, while other elements are regarded as minor components to improve the properties^[1,2]. Differing from the conventional one, a new alloy-design strategy was proposed by Cantor et al^[3] and Yeh et al^[4], which was called high-entropy alloys (HEAs) or multi-principal element alloys. At present, HEAs have become a new research hotspot in the field of materials science^[5-7].

A lot of researches about the effects of elemental additions in the AlCoCrFeNi alloy system have been done, for example, AlCoCrFeNiTi_x^[8], AlCoCrFeNiMo_x^[9], AlCoCrFeNiSi_x^[10], AlCoCrFeNiNb_x^[11], AlCoCrFeNiC_x^[12], AlCoCrFeNiV_x^[13] alloys and so on. However, in the AlCoCrFeNi alloy system, B element additions were little studied^[14].

In the present study, B was selected based on the following several reasons: firstly, B and many elements have very negative mixing enthalpies (the values of B and Co, B and Cr, B

and Fe, B and Ni atomic pairs are $-24, -31, -26$ and -24 kJ/mol, respectively)^[15,16], which would lead to the formation of borides, and the borides can improve the compression strength and wear resistance of alloys, such as CoCrCuFeNi-Al0.5B_x alloys^[17], AlTiNiMnB_x alloys^[18], Al0.5CoCrCuFeNiB_x alloys^[14] and FeCoNiCrCuTiMoAlSiB0.5 alloy^[19]; secondly, the atomic radius of B element is much smaller than that of other elements, which can make B atoms easy to diffuse during solidification. And diffusion is a key factor of controlling phase transition^[20]. The transition of the morphologies and microstructure is crucial to mechanical properties. Moreover, some alloys containing B element may possess good soft magnetic property^[21]. Therefore, in this paper, the effects of B element from $x=0$ to $x=1.0$ in molar fraction on the microstructures and properties of the AlCoCrFeNiB_x HEAs were investigated in detail.

1 Experiment

Received date: March 12, 2016

Foundation item: National Natural Science Foundation of China (51471044, 51671044); Dalian Youth Science and Technology Star Project Support Program (2016RQ005)

Corresponding author: Lu Yiping, Ph. D., Associate Professor, School of Materials Science and Engineering, Dalian University of Technology, Dalian 116024, P. R. China, Tel: 0086-411-84709400, E-mail: luyiping@dlut.edu.cn

Copyright © 2017, Northwest Institute for Nonferrous Metal Research. Published by Elsevier BV. All rights reserved.

The HEAs ingots of AlCoCrFeNiB_x ($x=0, 0.1, 0.25, 0.50, 0.75, 1.0$, denoted by B0, B0.1, B0.25, B0.5, B0.75 and B1.0, respectively) were prepared by vacuum arc furnace under a Ti-gettered high-purity argon atmosphere. The purity of all the raw materials (Al, Co, Cr, Fe, Ni, B) was above 99.9 wt%. The alloys were flipped and remelted at least five times. The button ingots ~ 30 g were directly solidified in a water-cooled cold copper hearth. X-ray diffractometer (XRD, Shimadzu XRD-6000) with Cu $K\alpha$ radiation was used for the phase analysis, and scanning angle ranged from 20° to 100° at a speed of $4^\circ/\text{min}$. Microstructures and phase compositions were observed by a scanning electron microscope with energy dispersive spectrometry (SEM, Zeiss supra55). The samples for the tests of compressive properties was made into $\Phi 5$ mm \times 10 mm, prepared from as-cast alloy button. The tests were conducted at a strain rate of $1.0\times 10^{-3}/\text{s}$. Vickers microhardness tester model (MH-60) with 1000 g for 15 s was used for hardness measurements. Five measurements were made for each sample to obtain the average experimental data. The magnetization curves were measured with JDM-13T vibrating sample magnetometer.

2 Results and Discussion

2.1 X-ray diffraction analysis

Fig.1 shows the XRD patterns of the AlCoCrFeNiB_x HEAs. When $x=0$, the alloy exhibits a B2 and bcc mixing structure. But when x exceeds 0.1, fcc phases begin to appear. And the intensities of fcc diffraction peaks increase as B contents increase, until B0.25. From B0.25, the intensities of both bcc and fcc phases begin to decrease as a result of the formation of borides, and distinct diffraction peaks of (Cr, Co)-borides could also be observed from Fig.1. Combined with the XRD diffraction patterns, a conclusion can be obtained that both Cr-borides and Co-borides are formed during $x=0.1\sim 0.25$.

2.2 Microstructure and characterization

Fig.2 and Fig.3 display the SEM images of the microstructures of the AlCoCrFeNiB_x HEAs. The morphologies of AlCoCrFeNiB_x HEAs are sensitive to alloying contents. B0

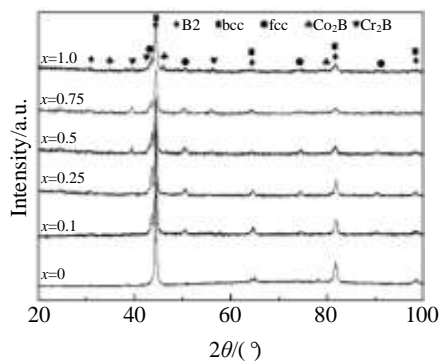


Fig.1 XRD patterns of the AlCoCrFeNiB_x HEAs ($x=0, 0.1, 0.25, 0.5, 0.75, 1.0$)

exhibits a typical equiaxed grain morphology, accompanying with obvious intragranular segregation, as shown in Fig.3a. The bright segregation area and the dark segregation area are denoted as A and B, respectively. The typical spinodal decomposition microstructure can be observed in the interior of the grains. According to the previous research^[22], the bright section and the dark section of interconnected microstructure are composed of (Fe, Co, Cr)-rich element and (Al, Ni)-rich element whereas section A has a higher amount of Al and Ni than section B.

When $x=0.1$, the alloy exhibits dendrite structures. The atomic radius of B element is far smaller than that of Al, Co, Cr, Fe and Ni elements, which may lead to the large strain energy of the crystal lattice when B atoms are further added. During the solidification, the B atoms are discharged in front of the solid-liquid surface to reduce the strain energy, which facilitates the constitutional undercooling that is beneficial to the formation of dendrites. The dendritic region is a mixture of rod-like and interlaced spinodal decomposition structures, marked by DA and DB, respectively. Their spinodal decomposition structure is composed of (Fe, Co, Cr)-rich elements and (Ni, Al)-rich elements, respectively^[23]. When $x=0.25$, the spinodal decomposition structures disappear completely. The change can be due to the high negative enthalpy of Cr-B, Co-B and Fe-B, and the formation of borides. According to the previous studies, the spinodal decomposition in AlCoCrFeNi HEAs system can be divided into two parts, one is rich in (Al, Ni), and the other is rich in (Fe, Co, Cr). But with B contents increasing, Cr and Co atoms tend to integrate with B to form borides, which breaks the composition of spinodal decomposition. As a result, the spinodal decomposition inside the grains disappears. From $x=0.5$, the needle-like structures appear in the region rich in (Al, Ni), as seen in Fig.3c. The interdendritic regions are mainly composed of both B and Cr elements. The reason is that Cr-B has a much lower mixing enthalpy (-31 kJ/mol) than among other elements^[23,24], which leads to the Cr and B atoms segregating together. Moreover, the interdendritic rod-like and long strips precipitates grow up, and connect together as B contents increase, as shown in Fig.3. When x exceeds 0.5, the interdendritic regions still consist of two parts, one is boride phase rich in Cr-B and Co-B, marked as S1, but the other part is rich-(Fe, Co, Cr) elements with the fcc solid solution structures, marked as S2. The interdendritic region of sample B1.0 can be divided into three parts. Combining the XRD patterns and EDS results (as seen in Table 1), it could be concluded that S1 and S3 are mainly composed of Cr borides and Co borides, respectively. And the S4 is rich-(Fe, Co) elements with bcc solid solution structures.

With the incorporation of B element, the grain size is refined obviously, such as sample B0, 200~300 μm , sample B0.1, 20~50 μm , until B0.75 and B1.0, 5~10 μm , as seen in Fig.2.

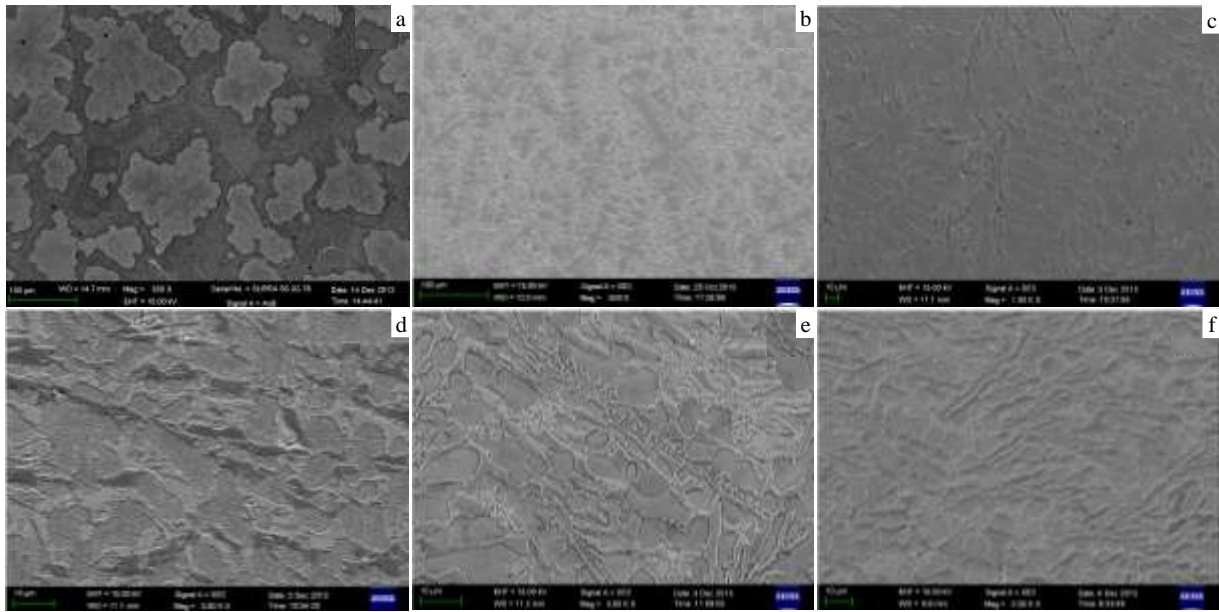


Fig.2 SEM images of AlCoCrFeNiB_x HEAs at low magnification: (a) $x=0$, (b) $x=0.1$, (c) $x=0.25$, (d) $x=0.5$, (e) $x=0.75$, and (f) $x=1.0$

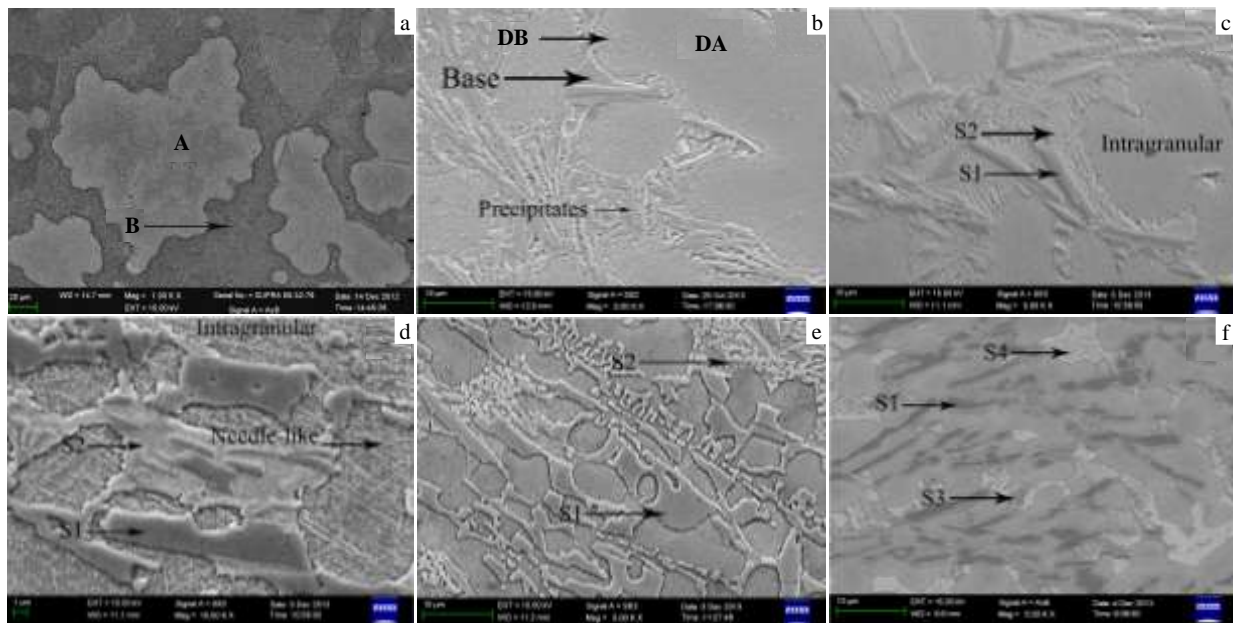


Fig.3 SEM images of AlCoCrFeNiB_x HEAs at high magnification: (a) $x=0$, (b) $x=0.1$, (c) $x=0.25$, (d) $x=0.5$, (e) $x=0.75$, and (f) $x=1.0$

2.3 Compressive properties

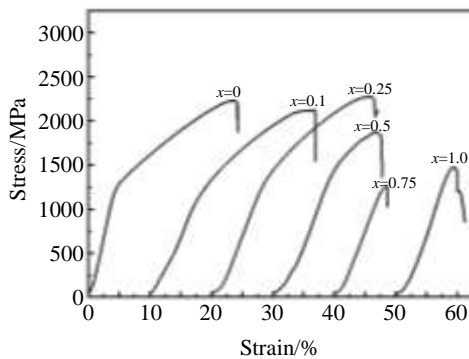
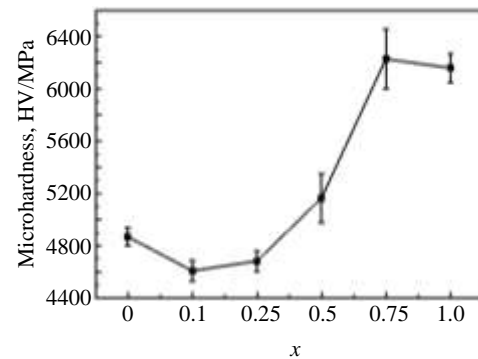
Fig.4 shows the compressive stress-strain curves of AlCo-CrFeNiB_x alloys with different B contents at the strain rate of $1.0 \times 10^{-3} \text{ s}^{-1}$. With B addition, the yield strength and fracture strength decrease obviously. When $x=0.75, 1.0$, even no yield stage exists any more, and the samples fracture during the elastic deformation. The compression ratio exhibits a trend of increasing from $x=0$ to $x=0.5$. When x exceeds 0.5, it shows a drastic decrease. When x reaches 0.75 and 1.0, the

compression ratios decrease to 8.7% and 11.3%, respectively.

As B contents increase, the compression strength and ratio of first increase and then decrease. The increase of compression ratios during $x=0 \sim 0.25$ can be attributed to the increasing volume fraction of fcc phases. According to the XRD and SEM results, much brittle borides form from $x=0.25$, and segregate in intergranular regions. The formation of brittle borides reduces the ductility and fracture strength of alloys, as shown in Fig.4.

Table 1 Chemical composition of AlCoCrFeNiB_x ($x=0, 0.1, 0.25, 0.5, 0.75, 1.0$) alloys (at%)

x		Al	Co	Cr	Fe	Ni	B	
0 ^[11]	Normal	20.0	20.0	20.0	20.0	20.0	0.0	
	Part A	24.0	19.8	16.5	17.5	22.2	0.0	
	Part B	1.1	19.1	46.9	28.2	4.6	0.0	
0.1	Normal	19.6	19.6	19.6	19.6	19.6	2.0	
	Dendrite	Part DA	30.6	17.9	11.2	15.4	25.0	0.0
		Part DB	22.9	19.3	18.1	19.5	20.1	0.0
	Interdendrite	Precipitates	1.1	3.8	33.3	6.8	1.7	53.3
		Base	11.2	22.0	25.5	26.4	14.9	0.0
0.25	Normal	19.0	19.0	19.0	19.0	19.0	5.0	
	Intragranular	Part DA	34.4	18.1	7.6	12.9	26.9	0.0
		Part DB	24.8	20.1	15.6	20.1	19.3	0.0
	Intergranular	S1	0.8	3.8	35.1	6.4	1.8	52.1
		S2	14.7	22.5	21.7	26.4	14.8	0.0
0.5	Normal	18.2	18.2	18.2	18.2	18.2	9.0	
	Intragranular	Needle-like	-	-	-	-	-	-
		Base	33.1	19.1	4.8	13.7	29.3	0.0
	Intergranular	S1	0.0	4.0	39.4	8.9	0.9	46.8
		S2	10.6	26.7	15.9	30.9	15.9	0.0
0.75	Normal	17.4	17.4	17.4	17.4	17.4	13.0	
	Intragranular		32.8	20.8	3.4	14.5	28.5	0.0
		S1	0.0	4.6	38.7	11.5	0.0	45.2
	Intergranular	S2	7.0	26.2	23.9	30.8	12.1	0.0
1.0	Normal	16.7	16.7	16.7	16.7	16.7	16.5	
	Intragranular		35.7	19.0	3.4	10.8	31.1	0.0
		S1	0.0	2.9	39.3	6.0	0.0	51.8
	Intergranular	S3	0.0	9.8	28.9	19.4	1.6	40.4
	S4	10.1	31.0	8.5	33.2	17.3	0.0	

Fig.4 Compressive properties of the AlCoCrFeNiB_x HEAs ($x=0, 0.1, 0.25, 0.5, 0.75, 1.0$)Fig.5 Vickers hardness curve of the AlCoCrFeNiB_x HEAs ($x=0, 0.1, 0.25, 0.5, 0.75, 1.0$)

2.4 Microhardness of AlCoCrFeNiB_x HEAs

Microhardness of AlCoCrFeNiB_x alloys are shown in Fig.5. All of the AlCoCrFeNiB_x HEAs possess high hardness. As B content increases from $x=0$ to $x=0.1$, the hardness HV declines from 4867 MPa to 4607 MPa, because the volume fraction of fcc phase increases and bcc phase drops with the addition of a small quantity of B element. (Fe, Co, Cr)-B has much lower mixing enthalpy than among other elements; therefore, large amounts of (Fe, Co, Cr) elements are attracted into interdendritic regions by B element. And the segregation of

(Fe, Co, Cr) leads to the formation and increase of fcc phase directly. When the value of x exceeds 0.1, the hardness begins to rise. This is attributed to the formation of hard borides which is favorable to the improvement of hardness. With B element addition, the borides begin to play a dominant role in the hardness instead of the bcc solid solutions phase and B2 phase. The alloy with a high content of B element $x=1$, shows the HV highest value of 6157 MPa. This change is consistent with the XRD and SEM analysis.

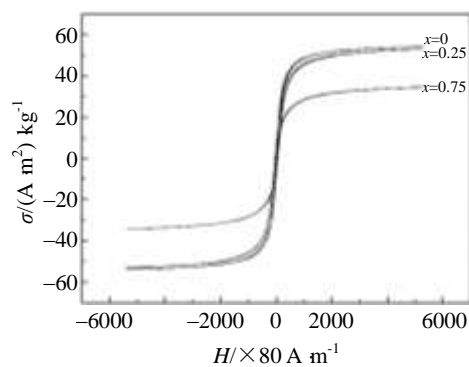


Fig.6 Magnetization curves of AlCoCrFeNiB_x HEAs (x=0, 0.25, 0.75)

2.5 Magnetic properties

The magnetic properties of AlCoCrFeNiB_x (x=0, 0.25, 0.75) HEAs were systematically investigated. The magnetization curves are shown in Fig.6. Obviously, all of the alloys show typical ferromagnetic behavior. The specific saturation magnetizations (σ) of B0, B0.25 and B0.75 alloys under the magnetic field of 4×10^5 A/m are 53.91, 34.64 and 34.27 (A m^2) kg^{-1} , respectively. The equation of the classification of magnetic properties is as follows^[25]:

$$\chi = \frac{M}{H} = \frac{\sigma\rho}{4\pi H} \quad (1)$$

where χ is the permeability, M (A/m) is the magnetization, H (A/m) is the magnetic field intensity, σ (A m^2) kg^{-1} is the specific saturation magnetization, ρ (g/cm^3) is the density of alloys.

As the B contents increase, the ferromagnetic behavior of alloys decreases obviously due to the addition of the non-magnetic B element into the alloy system. The coercive forces are 3.68×10^3 , 2.48×10^3 and 1.76×10^3 A/m for x=0, x=0.25, x=0.75, respectively, which reveals better and better soft magnetic behavior. When the content of B element increases, all alloys still exhibit ferromagnetic property, but the permeability shows a significant decrease, 5.8×10^{-3} , 3.6×10^{-3} and 3.5×10^{-3} , respectively, according to Eq.(1).

3 Conclusions

1) The AlCoCrFeNiB_x (x=0~1.0) HEAs are prepared by arc melting. As the B content increases, the structure of AlCoCrFeNiB_x (x=0~1.0) HEAs transforms from B2+bcc structure to B2+bcc+fcc structures, and finally forms B2+bcc+fcc+borides structures. The addition of B element facilitates the morphology changing from equiaxed-grains to dendrites when $x \leq 0.1$, accompanied with obvious refinement. Precipitated phase rich-(B, Cr) appears in the intergranular region, and gradually connects together.

2) A small quantity of B element addition can improve the strength and plasticity owing to the increased fcc solid solutions

structure. The strength and plasticity of alloys will decrease with the increased B elements. The samples even fracture during elastic deformation stage, due to the formation of borides.

3) With the increase of B elements, the hardness HV first declines to 4607 MPa, then increases to 6157 MPa. Because the fcc solid solution structures first increase, afterwards a lot of borides form with the addition of B elements. Coercive forces and the specific saturation magnetizations decrease distinctly, and the HEAs designed in the present paper show a better soft magnetic property with the increase of B element content.

References

- 1 Lin J P, Zhao L L, Chen Y G et al. *Intermetallics*[J], 2011, 19: 698
- 2 Haseeb, A S M A, Leng T S. *Intermetallics*[J], 2011, 19: 707
- 3 Cantor B, Chang I T H, Knight P et al. *Materials Science and Engineering A*[J], 2004, 375-377: 213
- 4 Yeh J W, Chen Y L, Lin S J et al. *Advanced Engineering Materials*[J], 2004, 6: 299
- 5 Zhang Y, Zuo T T, Tang Z et al. *Progress in Materials Science*[J], 2014, 64: 1
- 6 Gludovatz B, Hohenwarter A, Catoor D et al. *Science*[J], 2014, 345: 1153
- 7 Koželj P, Vrtnik S, Jelen A et al. *Physics Review Letter*[J], 2014, 113: 107 001
- 8 Zhou Y J, Zhang Y, Wang Y L et al. *Applied Physics Letter*[J], 2007, 90: 181904
- 9 Zhu J M, Fu H M, Zhang H F et al. *Materials Science and Engineering A*[J], 2010, 527: 6975
- 10 Zhu J M, Fu H M, Zhang H F et al. *Materials Science and Engineering A*[J], 2010, 527: 7210
- 11 Ma S G, Zhang Y. *Materials Science and Engineering A*[J], 2012, 532: 480
- 12 Zhu J M, Fu H M, Zhang H F et al. *Journal of Alloys and Compounds*[J], 2011, 509: 3476
- 13 Dong Y, Zhou K Y, Lu Y P et al. *Materials and Design*[J], 2014, 57: 67
- 14 Lee C P, Chen Y Y, Hsu C Y et al. *Journal of the Electrochemical Society*[J], 2007, 154: C424
- 15 Boer F R, Room R, Mattens W C M et al. *Cohesion in Metals*[M]. Amsterdam: Elsevier Science Publishing Company, 1989
- 16 Hsu C Y, Yeh J W, Chen S K et al. *Journal of the Electrochemical Society*[J], 2004, 35: 1465
- 17 Omer Dogan N, Benjamin Nielsen C, Jeffrey Hawk A. *Oxid Met*[J] 2013, 80: 177
- 18 Li C, Li J C, Zhao M et al. *Materials Science and Technology*[J], 2008, 24: 376
- 19 Zhang H, He Y Z, Pan Y. *Scripta Materialia*[J], 2013, 69: 342
- 20 Xu Z, Zhao L C. *Metal Solid State Phase Transition Principle* [M]. Beijing: Science Press, 2004 (in Chinese)
- 21 Sharma P, Zhang X, Zhang Y et al. *Journal of Applied Physics*[J], 2014, 115: 17

- 22 Wang F J, Zhang Y, Chen G L. *International Journal of Modern Physics B*[J], 2009, 23: 1254
- 23 Wang Y P, Li B S, Ren M X et al. *Materials Science and Engineering A*[J], 2008, 491: 154
- 24 Butvinová B, Butvin P, Matkoa I et al. *Applied Surface Science*[J], 2014, 23: 119
- 25 Ma S G, Zhang Y. *Materials Science and Engineering A*[J], 2012, 532: 480

AlCoCrFeNiB_x (x=0, 0.1, 0.25, 0.5, 0.75, 1.0) 高熵合金的微观结构与性能

陈秋实, 董 勇, 张峻嘉, 卢一平

(大连理工大学, 辽宁 大连 116024)

摘 要: 研究了硼元素对 AlCoCrFeNiB_x (x=0, 0.1, 0.25, 0.5, 0.75, 1.0, x 为摩尔百分比) 高熵合金微观组织和性能的影响。AlCoCrFeNi 高熵合金呈等轴晶结构, 晶内伴随着明显的成分偏析, 在等轴晶内可以观察到典型的调幅分解结构。然而, 当 x=0 时, 合金却转变为树枝晶结构。随着硼元素的进一步添加, 树枝晶以及调幅分解结构都开始逐渐消失, 并在晶体中形成大量的硼化物; 晶体结构也由 B2 + bcc 结构转变为 B2 + bcc + fcc 的混合结构, 最终转变为 B2 + bcc + fcc + 硼化物的混合结构; 合金硬度 HV 呈先降后升的趋势, 由 4860 MPa 降低至 4607 MPa, 最后又升高至 6157 MPa, 其中 x=0.1 时合金硬度最低; 抗压缩断裂强度呈明显的下降趋势, 在硼元素含量达到 0.75 时, 合金试样甚至在弹性变形阶段即发生了脆性断裂; 本系列合金均呈现软磁性, 其矫顽力和饱和磁化强度均随着硼元素含量的增加而下降, 而下降到矫顽力显示出硼元素对合金的软磁性有提高作用。

关键词: 高熵合金; 微观结构; 显微硬度; 压缩性能; 磁性能

作者简介: 陈秋实, 男, 1990 年生, 硕士, 大连理工大学材料科学与工程学院, 辽宁 大连 116024, 电话: 0411-84709400, E-mail: qiushilanzhe@126.com